

# A Bilayered Carbon with High Sunlight-Absorption Coefficient Designed by Flat-Band-Guided Strategy

Rui Xu, Hang Zhai, Di Wang, Xianqi Song, Dan Zhou,\* and Quan Li\*



Cite This: ACS Materials Lett. 2023, 5, 2747–2753



Read Online

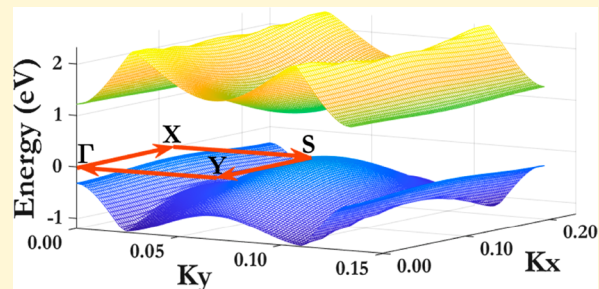
ACCESS |

Metrics & More

Article Recommendations

Supporting Information

**ABSTRACT:** The electronic band structure of a material determines its photovoltaic performance. In this work, we developed a methodology to explore desired semiconducting materials with a specialized designed fitness function for characterizing flat electronic bands via the generalization of our in-house-developed CALYPSO method. An intriguing bilayered carbon with  $sp^3$ - and  $sp^2$ -hybridized bonds, related to a bilayered reconstruction of (111) diamond or twisted graphene, was proposed and termed as two-dimensional diaphite. Two-dimensional diaphite has a direct electronic bandgap of 1.20 eV, with a high density of states near the band edges caused by the nearby flat bands, affording an extremely high sunlight-absorption coefficient. The type-II van der Waals heterojunctions composed of 2D diaphite and InSe monolayers yielded extraordinary performance for solar-to-electricity conversion with a theoretical power conversion efficiency of up to a record-breaking value of 24.1%, making it a potential candidate for high-efficiency and ultrathin photovoltaic devices. Our results show that the approach proposed herein is a feasible way of searching for functional semiconducting materials with specialized characteristic energy-band structures.



The goal of carbon neutrality with net-zero carbon dioxide emissions has sparked tremendous interest in renewable energy, such as sunlight, wind, geothermal energy, and nuclear power, which negligibly impact climate change. A solar cell is one of the most outstanding and successful examples of utilizing renewable energy that directly converts sunlight into electrical energy with a low-cost, clean, and sustainable supply through the photovoltaic effect.<sup>1–9</sup> Studies have shown that the single p-n junction cell can achieve maximum efficiency when the optimal electronic bandgap ( $E_{opt}$ ) of the sunlight-absorption material is 1.34 eV, according to the Shockley–Queisser limit.<sup>10,11</sup> The base component of most solar cells is bulk silicon,<sup>12</sup> which exhibits a satisfactory overall functional performance with a comprehensive consideration of efficiency, economy, and safety. However, the intrinsic optical properties of silicon with an indirect bandgap (1.1 eV) and a large energy difference with the direct gap (3.4 eV)<sup>13</sup> afford an imperfect optimum absorption coefficient and power conversion efficiency (PCE) in absorbing radiation from the visible range of electromagnetic radiation.

The intrinsic properties of two-dimensional (2D) semiconductors,<sup>14,15</sup> such as large specific surface area,<sup>16</sup> short migration distance,<sup>17</sup> unique electronic band structure,<sup>18</sup> high

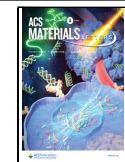
carrier mobility,<sup>19</sup> and high optical absorption coefficient in the solar wave range,<sup>20–24</sup> make them potential donors/acceptors to form type-II van der Waals heterojunctions in excitonic solar cells (XSCs) with high PCE. Various novel heterojunction structures with a donor bandgap of 1.0–1.7 eV and a small conduction band offset (0–0.3 eV) between the donor and acceptor ( $\Delta E_C$ ) have been proposed using structural design or high-throughput screening. Among them, the HfSe<sub>2</sub>/GeO<sub>2</sub> heterojunction has the previously largest known PCE value of 22.6%.<sup>25</sup>

As a congener of silicon, carbon produces various extraordinary 2D allotropes with different morphologies and advantageous properties due to its ability to form flexible and strong hybridized bonds, which are promising candidates for next-generation solar cell materials.<sup>26–28</sup> Although many 2D carbon candidates have been proposed via structural search<sup>29–31</sup> and high-throughput investigations<sup>32</sup> in the past

Received: June 27, 2023

Accepted: September 6, 2023

Published: September 8, 2023



ACS Publications

© 2023 American Chemical Society

decades, most of these structures exhibit unsatisfactory thermodynamic stability or inadequate functional performance.

The variation in the electronic band structure has been successfully used to explain a wide range of electrical characteristics and physical properties of functional materials, such as electrical resistivity and optical absorption. Bandgap engineering by efficient screening, controlling, or modulating the bandgap of materials has been widely applied as a powerful technique for reverse-designing novel photovoltaic materials and devices.<sup>33,34</sup> Recent studies have shown that certain materials possess flat electronic bands with a large density of states (DOS) near the conduction band minimum (CBM) and valence band maximum (VBM), affording highly probable optical transitions across the gap and excellent absorption coefficients and PCEs.<sup>35,36</sup> A pressing task is designing novel 2D carbon allotropes satisfying the electronic features, yielding excellent sunlight-adsorption efficiency, and generating underlying implications beyond the rational exploration and optimization of photovoltaic properties in a broad range of materials.

Herein, a specific design for an electronic flat-band-guided structure searching for desired semiconducting materials was conducted on 2D carbon structures through first-principles calculations combined with the particle swarm optimization (PSO) method. An intriguing bilayered carbon with  $sp^3$ - and  $sp^2$ -hybridized bonds, related to a bilayered reconstruction of (111) diamond or twisted graphene, was identified. This hybrid diamond-graphite structure was termed 2D diaphite. 2D diaphite possesses a direct electronic bandgap of 1.20 eV with a high DOS near the CBM and VBM caused by a nearby flat band, which explains its extremely high sunlight-absorption coefficient of  $>10^5$  cm<sup>-1</sup>. The absorption peak along the  $yy$  direction of the 2D diaphite could extensively cover the solar radiation spectrum. 2D diaphite forms compelling type-II van der Waals heterojunctions with InSe, CdSe, InS, and PtS monolayers, yielding extraordinary solar-to-electricity conversion with a record-breaking PCE of 24.1%, making it a promising candidate for applications in high-efficiency and ultrathin photovoltaic devices.

Structure searching proceeds through PSO<sup>37</sup> with an evolutionary algorithm implemented in the CALYPSO method,<sup>38</sup> a proven effective tool for structural design.<sup>39</sup> Instead of total energy, a specially designed fitness function, which quickly evolved in the direction of the optimal electronic bandgap with flat bands near the CBM and VBM, was applied for band characterization. As shown in Figure 1, two structures sharing identical standard bandgaps ( $E_{sd}$ ) but considerably different electronic DOS afford significant differences in their

photoelectric performances. Therefore, a specific energy width ( $E_{sp}$ ), the gap between the DOS values near the VBM and CBM that achieves the value of 0.3 states eV<sup>-1</sup> atom<sup>-1</sup> or the value of the integral achieves 0.3 states, considered for carbon allotropes, was defined to seek a proper balance between the bandgap and DOS for a better electronic description of given structures. The fitness function ( $F$ ) throughout the evolution of the PSO algorithm is defined as follows:

$$F = |E_{sd} - E_{opt}| + |E_{sp} - E_{opt}| \quad (1)$$

The first term of the formula is the energetic difference between the calculated standard electronic bandgap and optimal bandgap. The specific energy width quantifies the particular integral of the energy levels that can be occupied by electrons/holes, and thus, the second term is intended to allow the approach toward targeted structures with large density of electronic states. The fitness function is defined as sum of two terms and used to explore efficient sunlight-absorbing materials that exhibit flat electronic bands with a large DOS near the CBM and VBM. The accessible fitness function from first-principles calculations allows the users to perform an unbiased search of the energetically stable/metastable structures at given chemical compositions for both two- and three-dimensional materials. Unit cells containing up to 36 atoms were considered. The population size and number of generations were set at 30.

The structural relaxation and electronic structure calculations were conducted using density functional theory within the generalized gradient approximation with the Perdew–Burke–Ernzerhof (PBE) functional<sup>40</sup> for the exchange–correlation energy, as implemented in the Vienna Ab Initio Simulation Package code.<sup>41</sup> The Heyd–Scuseria–Ernzerhof (HSE06) function, mixing 25% of the nonlocal Hartree–Fock exchange and 75% of the semilocal exchange, was adopted to improve the calculation accuracy of the electronic and optical properties. The pseudopotentials of the all-electron projector augmented wave (PAW)<sup>42</sup> were adopted with the choice of four valence electrons ( $2s^22p^2$ ). The plane-wave kinetic energy cutoff of 600 eV for the plane-wave expansion and Monkhorst–Pack k-point mesh resolution of  $13 \times 13 \times 1$  in reciprocal space for all of the structures in the Brillouin zone were chosen to ensure an energy convergence and residual forces within 1 meV/atom and 1 meV/Å, respectively. As the GGA-PBE functional usually underestimates the electronic band gap, a bandgap of 1.0 eV was regarded as the primary screening index by the GGA-PBE functional. The computationally extremely expensive HSE06 calculations were performed to correct the band energies for the candidates. On the basis of convergence tests,  $19 \times 19 \times 1$  Monkhorst–Pack k-point meshes were chosen for the electronic band structures of 2D diaphite by the HSE06 hybrid functional to provide a better description of the band energies (especially the band positions). We showcased the 3D plots of the electronic band structures near the VBM and CBM, which are expected to have significant impact on the photovoltaic performance crucial to the applications. The x axis and y axis represent the  $K_x$  and  $K_y$  coordinates of the Brillouin zone, respectively, while the z axis represents the energy. The Graph Wavelet with Bayesian Structural Equation (GW+BSE) method<sup>43,44</sup> could also be adopted by our users for characterizing electronic bands, which is widely recognized as an accurate approach to describe the electronic and optical properties. The PHONOPY code was used to obtain the

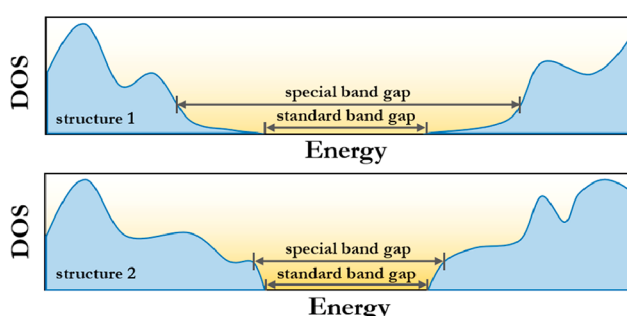


**Figure 1.** Sketch of DOS. Two structures sharing identical bandgaps but considerably different electronic DOS.

phonon frequencies.<sup>45</sup> The *ab initio* molecular dynamics (AIMD) calculation with a canonical ensemble (*NVT*) was used to prove the thermodynamic stability.

2D carbon structure searching was conducted for up to 36 carbon atoms and 3–5 Å thickness, and the structure was selected according to the bandgap and energy. Consequently, a 2D carbon structure with the *Pmmm* space group and  $D_{2h}$  point group was predicted. The primitive cell of this structure contained 24 carbon atoms, of which eight were  $sp^3$ -hybridized and 16 were  $sp^2$ -hybridized. The  $sp^3$ -hybridized carbon atoms possessed the structural characteristic of diamond, and the  $sp^2$ -hybridized carbon atoms formed graphite-like honeycomb structures, meaning that the structure contained the characteristic structures of diamond and graphite. Therefore, this 2D carbon structure was named 2D diaphite, and its top and side views are shown in Figure 2a. The lattice parameters of 2D

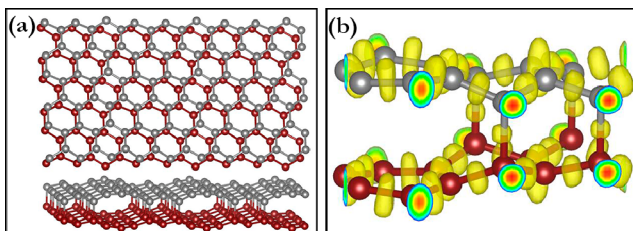


**Figure 2.** Structure and bonding of 2D diaphite. (a) Polyhedral views of 2D diaphite and (b) ELF of 2D diaphite with an isosurface level of 0.8.

diaphite are  $a = 7.435$  Å,  $b = 4.297$  Å, and  $c = 20.000$  Å, with a layer thickness of 2.881 Å. This study considered that the dehydrogenation of benzene and ethane could afford 2D

diaphite. In addition, other designed 2D carbon structures and their information are shown in Figure S1 and Table S1.

Furthermore, the electron localization function (ELF) was calculated and plotted to explore the bonding mechanism of 2D diaphite, as shown in Figure 2b. The level of the isosurface, considered the boundary of electron localization, was set at 0.75. Clearly, all the carbon bonds had electron localization, implying that they were bonded via covalent interactions

Stability is a prerequisite for applications of sunlight-absorption materials. Therefore, the phonon scattering spectrum was plotted to demonstrate the dynamic stability of the 2D diaphite, as shown in Figure 3a. All of the branches of the phonon scattering spectrum are positive, indicating that 2D diaphite was dynamically stable. Moreover, thermodynamic stability is important for applications of sunlight-absorption materials. Therefore, the AIMD simulation was processed using a  $4 \times 4$  2D diaphite supercell for 20 ps under 300 K. Based on the mean square displacement (MSD) of the AIMD simulation, clearly the 2D diaphite was thermodynamically stable at room temperature. Generally, the phonon spectra and AIMD calculations indicated that the 2D diaphite possessed dynamic and thermal stability.

As shown in Figure 3d, the bandgap and energy of 2D diaphite are compared with those of other 2D carbon structures, such as graphene,<sup>46</sup> graphyne,<sup>47</sup> PCF-graphene,<sup>48</sup> twin graphene,<sup>49</sup> net-H,<sup>50</sup> hP-C18,<sup>51</sup> hP-C23-2D,<sup>52</sup> egg-tray graphene H1 (H1), egg-tray graphene H2 (H2), egg-tray graphene T1 (T1), and egg-tray graphene T2 (T2),<sup>53</sup> to demonstrate the feasibility of 2D diaphite as a sunlight-absorption material.

Although the energy of the synthesized 2D diaphite was higher than that of graphene, it was lower than that of graphyne. 2D diaphite had a direct band gap closer to 1.34 eV than hP-C23-2D, T1, and T2. Additionally, 2D diaphite was

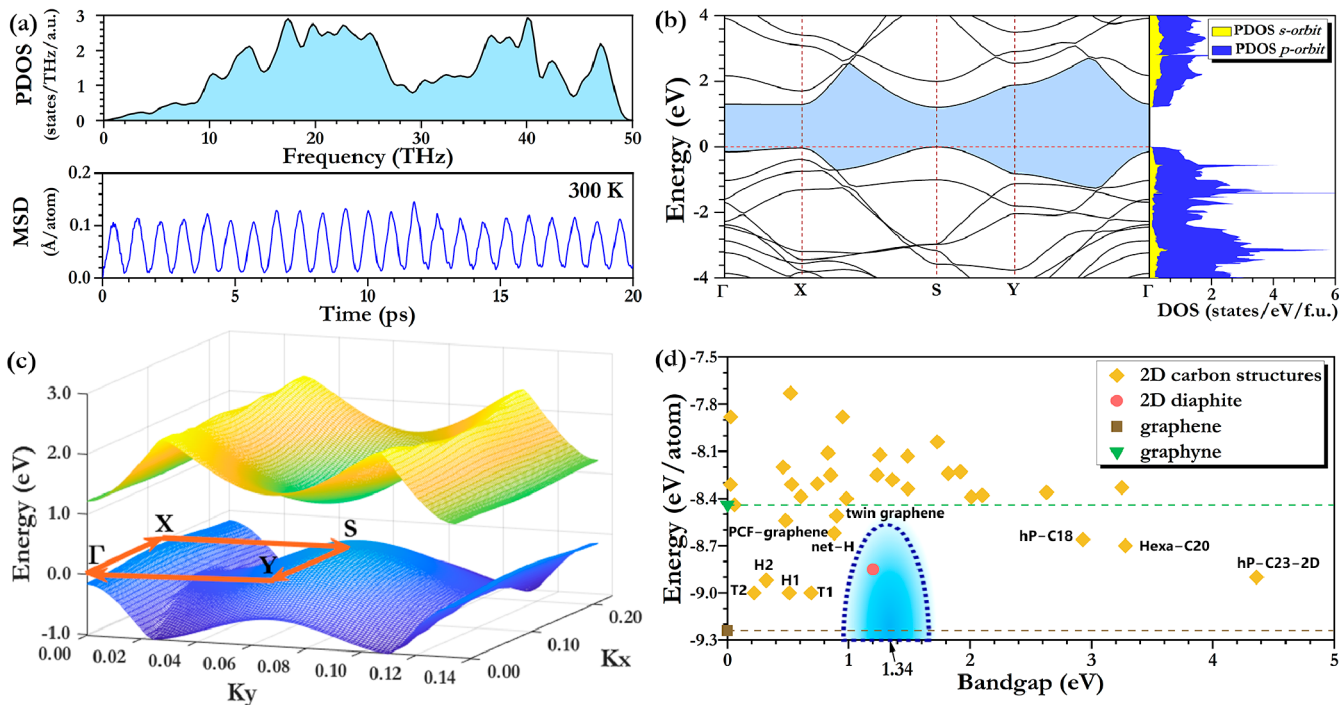


**Figure 3.** Stability and electronic properties. (a) Phonon scattering spectrum and MSD of 2D diaphite. (b) Band structure and DOS of 2D diaphite from HSE06 calculation. The Fermi level was set to zero. (c) 3D band structure of the VBM and CBM obtained using the HSE06 function. The orange arrows mark the path of the band. (d) Band gaps and energies of 2D carbon materials.

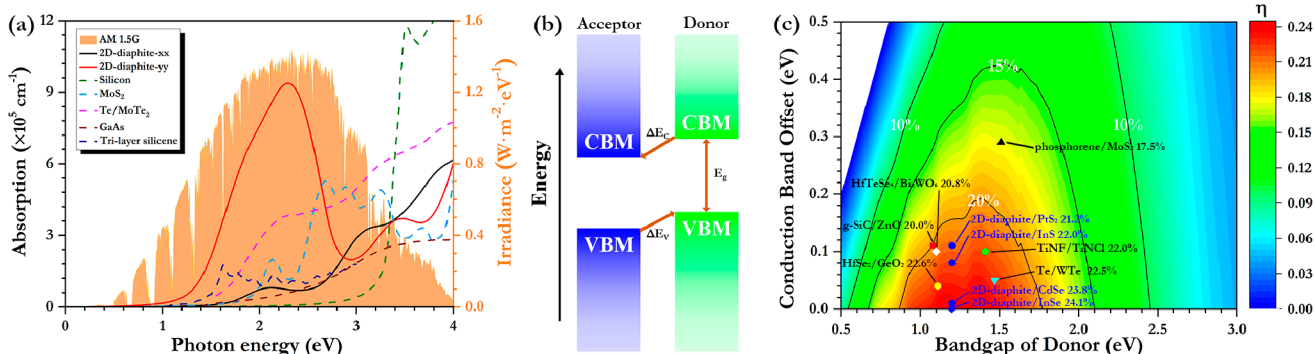


**Figure 4. Optical properties and applications.** (a) Absorption coefficients of 2D diaphite along the  $xx$  and  $yy$  directions and comparison with other solar cell materials. (b) Sketch map of type-II donor/acceptor band alignments. (c) Simulated PCE contours of the heterojunctions. Each point represents a type-II van der Waals heterojunction.

superior in energy to net-H, PCF-graphene, and twin graphene in energy. Comprehensively, 2D diaphite is more suitable for sunlight-absorption materials than other 2D carbon materials in terms of bandgap and energy. Furthermore, the band structure and the DOS were calculated and plotted to explore the electronic properties of 2D diaphite, as shown in Figure 3b. Clearly, 2D diaphite is a semiconductor with a direct bandgap of 1.20 eV at the S k point. The bandgap of 2D diaphite is near the optimal optical absorption bandgap of 1.34 eV, indicating that 2D diaphite is a promising candidate for applications in solar cells. It is abnormal that the VBM and CBM along the  $\Gamma$  to X point are flat. Therefore, the three-dimensional (3D) band structures of VBM and CBM were explored by plotting them, as shown in Figure 3c. A direct bandgap of 1.20 eV exists at the S point. Additionally, continuous bandgaps from 1.22 to 1.30 eV exist at the edge of the Brillouin zone along the  $\Gamma$  to X point, indicating that electron transition could occur simultaneously at the S point and at the edge of the Brillouin zone along the  $\Gamma$  to X point. Consequently, 2D diaphite has high sunlight-absorption properties due to its distinctive band structure.

The carrier mobility and concentration considerably influence the optical properties. However, there is a competitive relationship between carrier mobility and concentration. The carrier mobility and concentration determine the flow velocity of carriers and the total number of carriers, respectively. Additionally, the carrier mobility and concentration affect the electric current. Herein, the effective carrier mass and carrier mobility were calculated along different directions at room temperature (300 K) to explore the sunlight-absorption ability of the 2D diaphite. The effective masses of electrons and holes in 2D diaphite are  $0.75m_0$  and  $0.87m_0$ , respectively. Furthermore, the carrier mobility of 2D diaphite is 560–1386, comparable to that of the semiconductor materials with mature applications, as shown by the comparison in Table S2. However, 2D diaphite has a high carrier concentration due to the flat band and large DOS near the VBM and CBM, which is conducive to light-absorption properties. Thus, 2D diaphite is a promising sunlight-absorption material for photovoltaic devices.

The absorption of 2D diaphite was calculated and is shown in Figure 4a. In contrast with other sunlight-absorption materials, such as silicon,<sup>54</sup> MoS<sub>2</sub>,<sup>55</sup> Te/MoTe<sub>2</sub>,<sup>56</sup> GaAs,<sup>57</sup> and trilayer silicene,<sup>58</sup> 2D diaphite exhibited extremely high light absorption. Particularly, along the  $yy$  direction, the

absorption peak of  $9.14 \times 10^5 \text{ cm}^{-1}$  was at a 2.3 eV photon energy.

Additionally, the absorption peak of  $>10^5 \text{ cm}^{-1}$  along the  $xx$  direction was in the solar spectral irradiance range. Moreover, the absorption peak along the  $yy$  direction of 2D diaphite could cover almost the entire solar radiation spectrum, and the peak positions of the absorption and solar radiation spectra were very close (with reference to the AM 1.5G standard spectrum). Such a high light-absorption performance is due to the special band structure of 2D diaphite, especially the flat band from the high-symmetry point  $\Gamma$  to X. Thus, the extremely high absorption performance of 2D diaphite makes it a promising candidate for applications in photovoltaic devices.

Considering the direct bandgap of 1.20 eV and high light-absorption performance, 2D diaphite is a promising candidate as an XSC donor material. Thus, type-II van der Waals heterojunctions were designed to unearth the potential of 2D diaphite as a donor in XSCs. The band alignment sketch map of type-II van der Waals heterojunction is shown in Figure 4b. The upper limit of PCE was calculated in the limit of 100% external quantum efficiency using the following formula:<sup>59</sup>

$$\eta = \frac{0.65(E_g^d - \Delta E_c - 0.3) \int_{E_g^d}^{\infty} \frac{P(\hbar\omega)}{\hbar\omega} d(\hbar\omega)}{\int_0^{\infty} P(\hbar\omega) d(\hbar\omega)} \quad (2)$$

where 0.65 is the fill factor;  $E_g^d$  is the bandgap of the donor;  $\Delta E_c$  is the conduction band offset of the heterostructure, which should be positive for structuring type-II van der Waals heterojunctions; and  $P(\hbar\omega)$  is the AM 1.5G solar energy flux. Furthermore, the donor of type-II van der Waals heterojunctions should possess a bandgap close to 1.34 eV, and  $\Delta E_c$  should be small to make heterojunctions with high PCE. Therefore, acceptors having small  $\Delta E_c$  values with 2D diaphite should be found. The CBM and VBM of 2D diaphite were  $-4.31$  and  $-5.51$  eV with vacuum energy levels as a reference, respectively. Matching acceptors were found, and the VBM, CBM, and  $\Delta E_c$  of these materials are shown in Table 1. Subsequently, the PCEs of type-II acceptor/donor solar cells were estimated, as shown in Figure 4c. The PCEs of 2D diaphite/InSe, 2D diaphite/CdSe, 2D diaphite/InS, and 2D diaphite/PtS<sub>2</sub> were 24.1%, 23.8%, 22.0%, and 21.2%, respectively. Notably, the PCE of 2D diaphite/InSe exceeded the previous record-breaking PCE value for type-II van der Waals heterojunctions (HfSe<sub>2</sub>/GeO<sub>2</sub>,<sup>25</sup> 22.6%). The excellent photovoltaic characteristics of 2D diaphite show that the

**Table 1. CBMs and VBM of Acceptors and Their Conduction Band Offsets with 2D Diaphite**

	CBM (eV)	VBM (eV)	$\Delta E_c$ (eV)
InSe <sup>60</sup>	-4.31	-6.45	0.00
CdSe <sup>25</sup>	-4.32	-6.12	0.02
InS <sup>61</sup>	-4.39	-6.93	0.08
PtS <sub>2</sub> <sup>60,62</sup>	-4.42	-6.99	0.11

method of searching for light-absorbing materials described herein is desirable and effective.

In conclusion, a specific flat-band-guided structure search was processed, and a methodology to explore desired semiconducting materials with a specialized designed fitness function for characterizing flat electronic bands was developed. A 2D carbon structure with characteristic structures of diamond and graphite was predicted and termed as 2D diaphite. 2D diaphite possesses a direct bandgap of 1.2 eV, which is near the optimal optical absorption bandgap of 1.34 eV. 2D diaphite exhibits dynamic thermal stability. Notably, 2D diaphite possesses an extremely high absorption coefficient of  $>10^5 \text{ cm}^{-1}$ . Moreover, the absorption coefficient along the  $yy$  direction could match the solar radiation spectrum. Intriguingly, 2D diaphite forms compelling type-II van der Waals heterojunctions with InSe monolayers, making it a promising candidate for applications in high-efficiency and ultrathin photovoltaic devices. The current results of this study suggest that the described approach presents a feasible way of searching for functional semiconducting materials with specialized characteristic energy-band structures.

## ■ ASSOCIATED CONTENT

### SI Supporting Information

The Supporting Information is available free of charge at <https://pubs.acs.org/doi/10.1021/acsmaterialslett.3c00690>.

The designed two-dimensional carbon structures and their information, the AIMD and NEB calculations, and the electronic effective mass carrier mobility ([PDF](#))

## ■ AUTHOR INFORMATION

### Corresponding Authors

Dan Zhou – School of Physics, Changchun University of Science and Technology, Changchun 130022, China; Email: [zhoudan@cust.edu.cn](mailto:zhoudan@cust.edu.cn)

Quan Li – Key Laboratory of Material Simulation Methods & Software of Ministry of Education and State Key Lab of Superhard Materials, College of Physics, Jilin University, Changchun 130012, China; Jilin Provincial International Cooperation Key Laboratory of High-Efficiency Clean Energy Materials and International Center of Future Science, Jilin University, Changchun 130012, China; [orcid.org/0000-0002-7724-1289](#); Email: [liquan777@jlu.edu.cn](mailto:liquan777@jlu.edu.cn)

### Authors

Rui Xu – Key Laboratory of Material Simulation Methods & Software of Ministry of Education and State Key Lab of Superhard Materials, College of Physics, Jilin University, Changchun 130012, China; Jilin Provincial International Cooperation Key Laboratory of High-Efficiency Clean Energy Materials, Jilin University, Changchun 130012, China

Hang Zhai – Key Laboratory of Material Simulation Methods & Software of Ministry of Education and State Key Lab of Superhard Materials, College of Physics, Jilin University,

Changchun 130012, China; Jilin Provincial International Cooperation Key Laboratory of High-Efficiency Clean Energy Materials and International Center of Future Science, Jilin University, Changchun 130012, China

Di Wang – Key Laboratory of Material Simulation Methods & Software of Ministry of Education and State Key Lab of Superhard Materials, College of Physics, Jilin University, Changchun 130012, China; International Center of Future Science, Jilin University, Changchun 130012, China

Xianqi Song – Key Laboratory of Material Simulation Methods & Software of Ministry of Education and State Key Lab of Superhard Materials, College of Physics, Jilin University, Changchun 130012, China; International Center of Future Science, Jilin University, Changchun 130012, China; [orcid.org/0000-0002-4758-5865](#)

Complete contact information is available at:  
<https://pubs.acs.org/10.1021/acsmaterialslett.3c00690>

### Author Contributions

Q.L. designed the research and supervised the research. H.Z., D.W., X.S., and D.Z. coordinated the research. R.X. performed the structure searching and calculated the material properties. R.X. and Q.L. wrote the paper. All authors contributed to discussing the results and writing the paper. CRediT: Rui Xu Investigation, Methodology, Software, Investigation, Data curation, and Writing - original draft; Hang Zhai Investigation, and Validation; Di Wang Investigation, and Validation; Xianqi Song Investigation, Validation, and Writing - review and editing; Dan Zhou Investigation and Writing - review and editing; Quan Li Methodology, Resources, Writing - original draft, Writing - review and editing, and Funding acquisition. CRediT: Rui Xu data curation, investigation, methodology, software, writing-original draft; Hang Zhai investigation, validation; Di Wang investigation, validation; Xianqi Song investigation, validation, writing-review & editing; Dan Zhou investigation, writing-review & editing; Quan Li funding acquisition, methodology, resources, writing-original draft, writing-review & editing.

### Notes

The authors declare no competing financial interest.

## ■ ACKNOWLEDGMENTS

This work was supported by the National Key Research and Development Programs of China under Grants 2021YFA1400503 and 2018YFA0703400; the Natural Science Foundation of China under Grants T2325013, 52288102, 12074140, and 11704044; and the Program for the Jilin University (JLU) Science and Technology Innovative Research Team. The reported calculations utilized computing facilities at the High-Performance Computing Center of Jilin University.

## ■ REFERENCES

- Tan, S.; Huang, T.; Yavuz, I.; Wang, R.; Yoon, T.; Xu, M.; Xing, Q.; Park, K.; Lee, D. K.; Chen, C.-H.; Zheng, R.; Yoon, T.; Zhao, Y.; Wang, H. C.; Meng, D.; Xue, J.; Song, Y.; Pan, X.; Park, N. G.; Lee, J.-W.; Yang, Y. Stability-limiting Heterointerfaces of Perovskite Photovoltaics. *Nature* **2022**, *605*, 268–273.
- Kruitwagen, L.; Story, K.; Friedrich, J.; Byers, L.; Skillman, S.; Hepburn, C. A Global Inventory of Photovoltaic Solar Energy Generating Units. *Nature* **2021**, *598*, 604–610.
- Yang, S.; Chen, S.; Mosconi, E.; Fang, Y.; Xiao, X.; Wang, C.; Zhou, Y.; Yu, Z.; Zhao, J.; Gao, Y.; De Angelis, F.; Huang, J.

- Stabilizing Halide Perovskite Surfaces for Solar Cell Operation with Wide-Bandgap Lead Oxysalts. *Science* **2019**, *365*, 473–478.
- (4) Liu, D.; Luo, D.; Iqbal, A.; Orr, K.; Doherty, T.; Lu, Z.; Stranks, S.; Zhang, W. Strain Analysis and Engineering in Halide Perovskite Photovoltaics. *Nat. Mater.* **2021**, *20*, 1337–1346.
- (5) Geisz, J. F.; France, R. M.; Schulte, K. L.; Steiner, M. A.; Norman, A. G.; Guthrey, H. L.; Young, M. R.; Song, T.; Moriarty, T. Six-Junction III-V Solar Cells with 47.1% Conversion Efficiency Under 143 Suns Concentration. *Nat. Energy* **2020**, *5*, 326–335.
- (6) Fang, Z.; Wang, L.; Mu, X.; Chen, B.; Xiong, Q.; Wang, W.; Ding, J.; Gao, P.; Wu, Y.; Cao, J. Grain Boundary Engineering with Self-Assembled Porphyrin Supramolecules for Highly Efficient Large-Area Perovskite Photovoltaics. *J. Am. Chem. Soc.* **2021**, *143*, 18989–18996.
- (7) Shao, S.; Cui, X.; Li, Z. Recent Progress in Understanding the Structural, Optoelectronic, and Photophysical Properties of Lead Based Dion-Jacobson Perovskites as Well as Their Application in Solar Cells. *ACS Mater. Lett.* **2022**, *4*, 891–917.
- (8) Ge, S.; Xu, H.; Wang, T.; Gu, E.; Lin, X.; Yang, G. 9.2% Efficient Cu<sub>2</sub>ZnSn (S, Se)<sub>4</sub> Thin Film Solar Cell Based on Inkjet-Printed Absorber. *ACS Mater. Lett.* **2023**, *5*, 1767–1771.
- (9) Gil-Escríg, L.; Hu, S.; Zanoni, K. P.; Paliwal, A.; Hernández-Fenollosa, M. A.; Roldán-Carmona, C.; Sessolo, M.; Wakamiya, A.; Bolink, H. J. Perovskite/Perovskite Tandem Solar Cells in the Substrate Configuration with Potential for Bifacial Operation. *ACS Mater. Lett.* **2022**, *4*, 2638–2644.
- (10) Shockley, W.; Queisser, H. Detailed Balance Limit of Efficiency of P-N Junction Solar Cells. *J. Appl. Phys.* **1961**, *32*, 510–519.
- (11) Yu, L.; Zunger, A. Identification of Potential Photovoltaic Absorbers Based on First-Principles Spectroscopic Screening of Materials. *Phys. Rev. Lett.* **2012**, *108*, 068701.
- (12) Jelle, B. P.; Breivik, C.; Rønne, H. D. Building Integrated Photovoltaic Products: A State-of-The-Art Review and Future Research Opportunities. *Sol. Energy Mater. Sol. Cells* **2012**, *100*, 69–96.
- (13) Hybertsen, M. S.; Louie, S. G. First-Principles Theory of Quasiparticles: Calculation of Band Gaps in Semiconductors and Insulators. *Phys. Rev. Lett.* **1985**, *55*, 1418.
- (14) Chen, J.; Lin, S.; Xu, M.; Wang, F.; Shao, Y.; Hao, J.; Li, Y. Metal-Decoration-Free Li<sub>3</sub>C<sub>2</sub> Monolayer with Heptacoordinate Carbons as a Promising Hydrogen Storage Medium. *ACS Mater. Lett.* **2022**, *4*, 1402–1410.
- (15) Zhang, Y.; Yuan, X.; Hao, J.; Xu, M.; Li, Y. Realizing High-Temperature Superconductivity in Borophene with Dirac States Assembled by Kagome and Honeycomb Boron Layers. *Mater. Today Phys.* **2023**, *35*, 101144.
- (16) Zhang, P.; Wang, M.; Liu, Y.; Yang, S.; Wang, F.; Li, Y.; Chen, G.; Li, Z.; Wang, G.; Zhu, M.; Dong, R.; Yu, M.; Schmidt, O.; Feng, X. Dual-Redox-Sites Enable Two-Dimensional Conjugated Metal-Organic Frameworks with Large Pseudocapacitance and Wide Potential Window. *J. Am. Chem. Soc.* **2021**, *143*, 10168–10176.
- (17) Ju, L.; Shang, J.; Tang, X.; Kou, L. Tunable Photocatalytic Water Splitting by The Ferroelectric Switch in A 2D AgBiP<sub>2</sub>Se<sub>6</sub> Monolayer. *J. Am. Chem. Soc.* **2020**, *142*, 1492–1500.
- (18) Xia, F.; Wang, H.; Xiao, D.; Dubey, M.; Ramasubramanian, A. Two-Dimensional Material Nanophotonics. *Nat. Photonics* **2014**, *8*, 899–907.
- (19) Niu, W.; Ma, J.; Soltani, P.; Zheng, W.; Liu, F.; Popov, A.; Weigand, J.; Komber, H.; Poliani, E.; Casiraghi, C.; Droste, J.; Hansen, M.; Osella, S.; Beljonne, D.; Bonn, M.; Wang, H.; Feng, X.; Liu, J.; Mai, Y. A Curved Graphene Nanoribbon with Multi-Edge Structure and High Intrinsic Charge Carrier Mobility. *J. Am. Chem. Soc.* **2020**, *142*, 18293–18298.
- (20) Li, X.; Guan, Y.; Li, X.; Fu, Y. Stereochemically Active Lone Pairs and Nonlinear Optical Properties of Two-Dimensional Multilayered Tin and Germanium Iodide Perovskites. *J. Am. Chem. Soc.* **2022**, *144*, 18030–18042.
- (21) Gao, L.; Li, X.; Traore, B.; Zhang, Y.; Fang, J.; Han, Y.; Even, J.; Katan, C.; Zhao, K.; Liu, S.; Kanatzidis, M. m-Phenylenediammonium as A New Spacer for Dion-Jacobson Two-Dimensional Perovskites. *J. Am. Chem. Soc.* **2021**, *143*, 12063–12073.
- (22) Zhao, Y.; Qiu, Y.; Feng, J.; Zhao, J.; Chen, G.; Gao, H.; Zhao, Y.; Jiang, L.; Wu, Y. Chiral 2D-Perovskite Nanowires for Stokes Photodetectors. *J. Am. Chem. Soc.* **2021**, *143*, 8437–8445.
- (23) Cao, J.; Duan, C.; Li, Z.; Jin, B.; Li, J.; Wan, L.; Zhao, L.; Dong, B.; Wu, C. Theoretical Selection of 2D Perovskite for Constructing Efficient Heterojunction Solar Cells. *ACS Mater. Lett.* **2023**, *5*, 970–978.
- (24) Qin, Z.; Chen, Y.; Zhu, K.; Zhao, Y. Two-Dimensional Materials for Perovskite Solar Cells with Enhanced Efficiency and Stability. *ACS Mater. Lett.* **2021**, *3*, 1402–1416.
- (25) Linghu, J.; Yang, T.; Luo, Y.; Yang, M.; Zhou, J.; Shen, L.; Feng, Y. P. High-Throughput Computational Screening of Vertical 2D Van Der Waals Heterostructures for High-Efficiency Excitonic Solar Cells. *ACS Appl. Mater. Interfaces* **2018**, *10*, 32142–32150.
- (26) Belin, T.; Epron, F. Characterization Methods of Carbon Nanotubes: A Review. *Mater. Sci. Eng., B* **2005**, *119*, 105–118.
- (27) Wu, Y. H.; Yu, T.; Shen, Z. X. Two-Dimensional Carbon Nanostructures: Fundamental Properties, Synthesis, Characterization, and Potential Applications. *J. Appl. Phys.* **2010**, *108*, 071301.
- (28) Hirsch, A. The Era of Carbon Allotropes. *Nat. Mater.* **2010**, *9*, 868–871.
- (29) Lu, S.; Wang, Y.; Liu, H.; Miao, M. S.; Ma, Y. Self-Assembled Ultrathin Nanotubes on Diamond (100) Surface. *Nat. Commun.* **2014**, *5*, 3666.
- (30) Yin, H.; Shi, X.; He, C.; Martinez-Canales, M.; Li, J.; Pickard, C. J.; Tang, C.; Ouyang, T.; Zhang, C.; Zhong, J. Stone-Wales Graphene: A Two-Dimensional Carbon Semimetal with Magic Stability. *Phys. Rev. B* **2019**, *99*, 041405.
- (31) Zhou, N.; Zhou, P.; Li, J.; He, C.; Zhong, J. Si-Cmma: A Silicon Thin Film with Excellent Stability and Dirac Nodal Loop. *Phys. Rev. B* **2019**, *100*, 115425.
- (32) Kabiraj, A.; Kumar, M.; Mahapatra, S. High-Throughput Discovery of High Curie Point Two-Dimensional Ferromagnetic Materials. *npj Comput. Mater.* **2020**, *6*, 35.
- (33) Wang, Q.; Xu, B.; Sun, J.; Liu, H.; Zhao, Z.; Yu, D.; Fan, C.; He, J. Direct Band Gap Silicon Allotropes. *J. Am. Chem. Soc.* **2014**, *136*, 9826–9829.
- (34) Oganov, A. R.; Pickard, C. J.; Zhu, Q.; Needs, R. J. Structure Prediction Drives Materials Discovery. *Nat. Rev. Mater.* **2019**, *4*, 331–348.
- (35) Xiao, Z.; Meng, W.; Saparov, B.; Duan, H. S.; Wang, C.; Feng, C.; Liao, W.; Ke, W.; Zhao, D.; Wang, J.; Mitzi, D. B.; Yan, Y. Photovoltaic Properties of Two-Dimensional (CH<sub>3</sub>NH<sub>3</sub>)<sub>2</sub>Pb(SCN)<sub>2</sub>I<sub>2</sub> Perovskite: A Combined Experimental and Density Functional Theory Study. *J. Phys. Chem. Lett.* **2016**, *7*, 1213–1218.
- (36) Xia, C.; Du, J.; Xiong, W.; Jia, Y.; Wei, Z.; Li, J. A Type-II GeSe/Sns Heterobilayer with A Suitable Direct Gap, Superior Optical Absorption and Broad Spectrum for Photovoltaic Applications. *J. Mater. Chem. A* **2017**, *5*, 13400–13410.
- (37) Kennedy, J.; Eberhart, R. Particle Swarm Optimization. In *Proceedings of International Conference on Neural Networks (ICNN'95)*, Perth, Australia, 1995; IEEE, 1995; pp 1942–1948.
- (38) Wang, Y.; Lv, J.; Zhu, L.; Ma, Y. CALYPSO: A Method for Crystal Structure Prediction. *Comput. Phys. Commun.* **2012**, *183*, 2063.
- (39) Gao, B.; Gao, P.; Lu, S.; Lv, J.; Wang, Y.; Ma, Y. Interface Structure Prediction via CALYPSO Method. *Sci. Bull.* **2019**, *64*, 301–309.
- (40) Perdew, J. P.; Burke, K.; Ernzerhof, M. Generalized Gradient Approximation Made Simple. *Phys. Rev. Lett.* **1996**, *77*, 3865–3868.
- (41) Kresse, G.; Furthmüller, J. Efficient Iterative Schemes for *ab initio* Total-Energy Calculations Using a Plane-Wave Basis Set. *Phys. Rev. B* **1996**, *54*, 11169.
- (42) Becke, A. D. Density-Functional Exchange-Energy Approximation with Correct Asymptotic Behavior. *Phys. Rev. A* **1988**, *38*, 3098.

- (43) Onida, G.; Reining, L.; Rubio, A. Electronic Excitations: Density-Functional Versus Many-Body Green's-Function Approaches. *Rev. Mod. Phys.* **2002**, *74*, 601–659.
- (44) Rohlfing, M.; Louie, S. G. Electron-Hole Excitations and Optical Spectra from First Principles. *Phys. Rev. B* **2000**, *62*, 4927–4944.
- (45) Togo, A.; Tanaka, I. First Principles Phonon Calculations in Materials Science. *Scr. Mater.* **2015**, *108*, 1–5.
- (46) Novoselov, K. S.; Geim, A. K.; Morozov, S. V.; Jiang, D.; Zhang, Y.; Dubonos, S. V.; Grigorieva, I. V.; Firsov, A. A. Electric Field Effect in Atomically Thin Carbon Films. *Science* **2004**, *306*, 666–669.
- (47) Narita, N.; Nagai, S.; Suzuki, S.; Nakao, K. Optimized Geometries and Electronic Structures of Graphyne and Its Family. *Phys. Rev. B* **1998**, *58*, 11009.
- (48) Shen, Y.; Yu, J.; Liu, J.; Guo, Y.; Qie, Y.; Wang, Q. PCF-Graphene: A 2D sp<sup>2</sup>-Hybridized Carbon Allotrope with a Direct Band Gap. *J. Phys. Chem. C* **2019**, *123*, 4567–4573.
- (49) Jiang, J. W. J.; Leng, T.; Li, J. X.; Guo, Z. R.; Chang, T. C.; Guo, X. M.; Zhang, T. Y. Twin Graphene: A Novel Two-Dimensional Semiconducting Carbon Allotrope. *Carbon* **2017**, *118*, 370–375.
- (50) Hu, M.; Shu, Y.; Cui, L.; Xu, B.; Yu, D.; He, J. Theoretical Two-Atom Thick Semiconducting Carbon Sheet. *Phys. Chem. Chem. Phys.* **2014**, *16*, 18118–18123.
- (51) Wang, S.; Li, J.; Zhu, X.; Wang, M. A New Two-Dimensional Semiconducting Carbon Allotrope: A First-Principles Study. *Carbon* **2019**, *143*, 517–522.
- (52) Lu, Y.; Zhu, X.; Wang, M. Theoretical Investigations of a New Two-Dimensional Carbon Allotrope: hP-C23-2D. *Comput. Mater. Sci.* **2019**, *167*, 8–12.
- (53) Liu, W.; Zhao, L.; Zurek, E.; Xia, J.; Zheng, Y.; Lin, H.; Liu, J.; Miao, M. Building Egg-Tray-Shaped Graphenes That Have Superior Mechanical Strength and Band Gap. *npj Comput. Mater.* **2019**, *5*, 71.
- (54) Jellison, G., Jr.; Modine, F. Optical Constants for Silicon at 300 and 10 K Determined from 1.64 to 4.73 eV by Ellipsometry. *J. Appl. Phys.* **1982**, *53*, 3745–3753.
- (55) Ullah, M. S.; Yousuf, A. H. B.; Es-Sakhi, A. D.; Chowdhury, M. H. Analysis of optical and electronic properties of MoS<sub>2</sub> for optoelectronics and FET applications. *AIP Conf. Proc.* **2018**, *1957*, 020001.
- (56) Wu, K.; Ma, H.; Gao, Y.; Hu, W.; Yang, J. Highly-Efficient Heterojunction Solar Cells Based on Two-Dimensional Tellurene and Transition Metal Dichalcogenides. *J. Mater. Chem. A* **2019**, *7*, 7430–7436.
- (57) Sturge, M. Optical Absorption of Gallium Arsenide between 0.6 And 2.75 eV. *Phys. Rev.* **1962**, *127*, 768.
- (58) Lv, J.; Xu, M.; Lin, S.; Shao, X.; Zhang, X.; Liu, Y.; Wang, Y.; Chen, Z.; Ma, Y. Direct-Gap Semiconducting Tri-Layer Silicene with 29% Photovoltaic Efficiency. *Nano Energy* **2018**, *51*, 489–495.
- (59) Scharber, M. C.; Mühlbacher, D.; Koppe, M.; Denk, P.; Waldauf, C.; Heeger, A. J.; Brabec, C. J. Design Rules for Donors in Bulk-heterojunction Solar Cells—Towards 10% Energy-conversion Efficiency. *Adv. Mater.* **2006**, *18*, 789–794.
- (60) Rasmussen, F. A.; Thygesen, K. S. Computational 2D Materials Database: Electronic Structure of Transition-Metal Dichalcogenides and Oxides. *J. Phys. Chem. C* **2015**, *119*, 13169–13183.
- (61) Zhuang, H. L.; Hennig, R. G. Single-Layer Group-III Monochalcogenide Photocatalysts for Water Splitting. *Chem. Mater.* **2013**, *25*, 3232–3238.
- (62) Zhuang, H. L.; Hennig, R. G. Computational Search for Single-Layer Transition-Metal Dichalcogenide Photocatalysts. *J. Phys. Chem. C* **2013**, *117*, 20440–2044.

# A bilayered carbon with high sunlight-absorption coefficient designed by flat-band-guided strategy

Rui Xu,<sup>a, b</sup> Hang Zhai,<sup>a, b, c</sup> Di Wang,<sup>a, c</sup> Xianqi Song,<sup>a, c</sup> Dan Zhou,<sup>d,\*</sup> and Quan Li<sup>a, b, c, \*</sup>

<sup>a</sup> Key Laboratory of Material Simulation Methods & Software of Ministry of Education and State Key Lab of Superhard Materials, College of Physics, Jilin University, Changchun 130012, China.

<sup>b</sup>Jilin Provincial International Cooperation Key Laboratory of High-Efficiency Clean Energy Materials, Jilin University, Changchun 130012, China.

<sup>c</sup>International Center of Future Science, Jilin University, Changchun 130012, China.

<sup>d</sup>School of Physics, Changchun University of Science and Technology, Changchun 130022, China

\* zhoudan@cust.edu.cn

\* liquan777@jlu.edu.cn

Figure S1. The designed two-dimensional carbon structures	1
Figure S2. The AIMD calculation	2
Figure S3. The energy barrier	2
Table S1 The information designed two-dimensional carbon structures	3
Table S2. The electronic effective masscarrier mobility	7
Reference	7

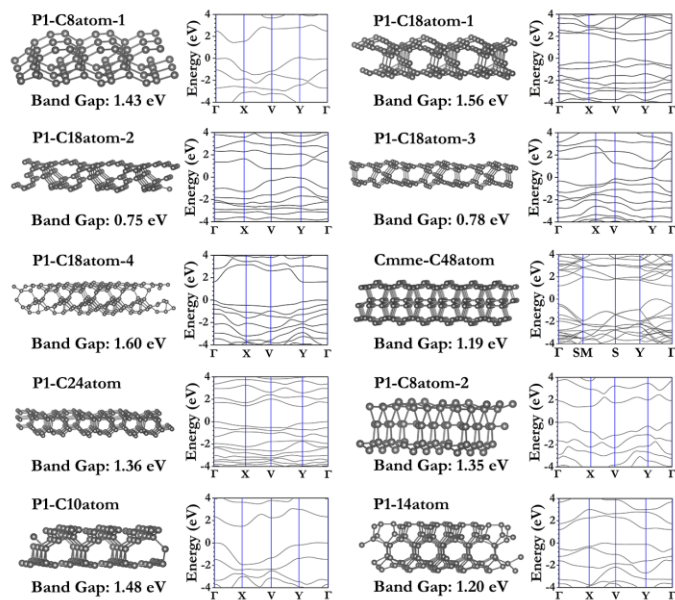


**Figure S1. The designed two-dimensional (2D) carbon structures could exhibit high efficiency for solar cells and their band structure by using HSE06 function.**

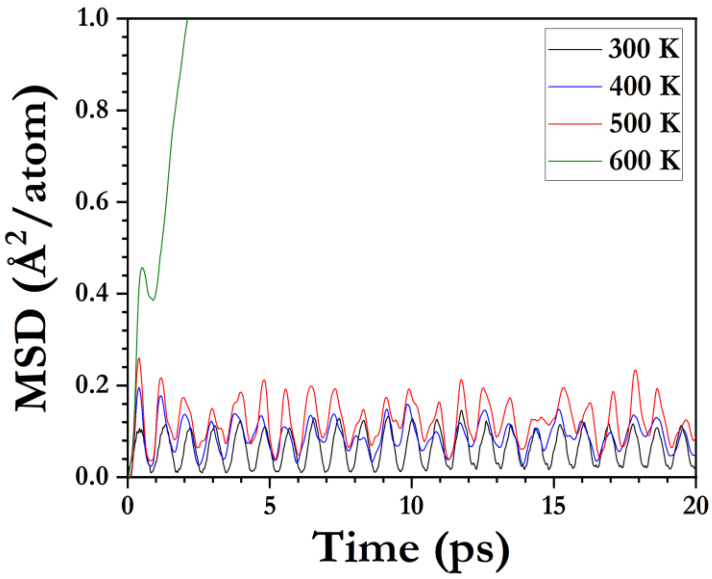


**Figure S2.** The mean squared displacements of atomic positions versus time for the 2D diaphite at elevated temperature. The MSD values of the carbon atoms remain nearly constant at 500 K, suggesting that the structural motif is dynamically stable with all atoms near the equilibrium, while it is unstable above 600 K as MSD values begin to rapid increase.

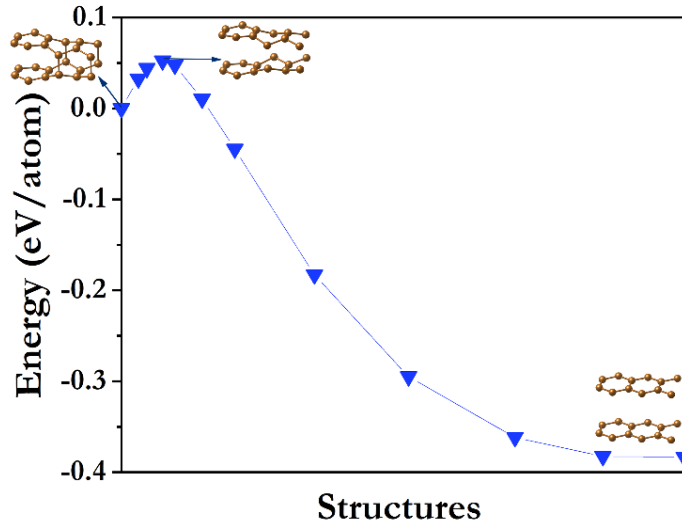


**Figure S3.** The activation barrier has been evaluated in the conversion process from the 2D diaphite to bilayer graphene using Nudged Elastic Band calculations (NEB). The results show the energy change along the transformation pathway. The theoretical barrier is calculated to be 0.052 eV/atom that is not easy to be overcame and ensured 2D diaphite to avoid the spontaneous splitting into bilayer graphene.

**Table S1: The information designed two-dimensional carbon structures.**

2D carbon structure	Space group	Energy	Lattice parameters	Wyckoff position
P1-C8atom-1	<i>P1</i>	-8.25 eV	$a= 3.717 \text{ \AA}$ $b= 3.732 \text{ \AA}$ $c= 24.684 \text{ \AA}$ $\alpha= 91.819^\circ$ $\beta= 93.928^\circ$ $\gamma= 100.449^\circ$	1a (0.429, 0.706, 0.456) 1a (0.048, 0.699, 0.463) 1a (0.010, 0.008, 0.493) 1a (0.677, 0.469, 0.459) 1a (0.404, 0.475, 0.559) 1a (0.398, 0.800, 0.562) 1a (0.356, 0.123, 0.531) 1a (0.639, 0.094, 0.479)
P1-C18atom-1	<i>P1</i>	-8.14 eV	$a= 4.879 \text{ \AA}$ $b= 5.488 \text{ \AA}$ $c= 23.998 \text{ \AA}$ $\alpha= 90.830^\circ$ $\beta= 93.055^\circ$ $\gamma= 64.691^\circ$	1a (0.572, 0.609, 0.525) 1a (0.238, 0.370, 0.546) 1a (0.184, 0.141, 0.463) 1a (0.869, 0.848, 0.560) 1a (0.451, 0.655, 0.416) 1a (0.733, 0.179, 0.420) 1a (0.744, 0.445, 0.408) 1a (0.410, 0.931, 0.424) 1a (0.952, 0.059, 0.538) 1a (0.055, 0.418, 0.431) 1a (0.386, 0.467, 0.504) 1a (0.570, 0.847, 0.541) 1a (0.075, 0.595, 0.573) 1a (0.271, 0.093, 0.533) 1a (0.727, 0.328, 0.518) 1a (0.253, 0.536, 0.444) 1a (0.905, 0.123, 0.474) 1a (0.601, 0.023, 0.405)
P1-C18atom-2	<i>P1</i>	-8.39 eV	$a= 5.636 \text{ \AA}$ $b= 6.271 \text{ \AA}$ $c= 25.205 \text{ \AA}$ $\alpha= 101.838^\circ$ $\beta= 95.760^\circ$ $\gamma= 63.397^\circ$	1a (0.693, 0.832, 0.477) 1a (0.015, 0.397, 0.453) 1a (0.222, 0.969, 0.436) 1a (0.283, 0.865, 0.554) 1a (0.839, 0.592, 0.498) 1a (0.748, 0.223, 0.478) 1a (0.259, 0.386, 0.441) 1a (0.814, 0.986, 0.498) 1a (0.683, 0.476, 0.518) 1a (0.039, 0.642, 0.536) 1a (0.324, 0.066, 0.566) 1a (0.289, 0.482, 0.556) 1a (0.991, 0.184, 0.448)

				$1a$ (0.463, 0.880, 0.446)
				$1a$ (0.502, 0.297, 0.446)
				$1a$ (0.034, 0.863, 0.532)
				$1a$ (0.334, 0.262, 0.566)
				$1a$ (0.466, 0.597, 0.551)
P1-C18atom-3	<i>P1</i>	-8.31 eV	$a= 3.661 \text{ \AA}$	$1a$ (0.779, 0.618, 0.493)
			$b= 7.150 \text{ \AA}$	$1a$ (0.056, 0.813, 0.569)
			$c= 23.975 \text{ \AA}$	$1a$ (0.385, 0.678, 0.567)
			$\alpha= 97.359^\circ$	$1a$ (0.450, 0.569, 0.456)
			$\beta= 91.945^\circ$	$1a$ (0.686, 0.773, 0.544)
			$\gamma= 82.083^\circ$	$1a$ (0.083, 0.666, 0.461)
				$1a$ (0.277, 0.131, 0.549)
				$1a$ (0.658, 0.979, 0.459)
				$1a$ (0.006, 0.837, 0.444)
				$1a$ (0.010, 0.003, 0.556)
				$1a$ (0.938, 0.113, 0.448)
				$1a$ (0.195, 0.334, 0.549)
				$1a$ (0.454, 0.474, 0.553)
				$1a$ (0.790, 0.303, 0.463)
				$1a$ (0.630, 0.993, 0.531)
				$1a$ (0.249, 0.981, 0.440)
				$1a$ (0.528, 0.390, 0.430)
				$1a$ (0.825, 0.418, 0.522)
P1-C18atom-4	<i>P1</i>	-8.34 eV	$a= 4.380 \text{ \AA}$	$1a$ (0.396, 0.111, 0.573)
			$b= 5.291 \text{ \AA}$	$1a$ (0.281, 0.580, 0.407)
			$c= 21.868 \text{ \AA}$	$1a$ (0.089, 0.377, 0.543)
			$\alpha= 90.635^\circ$	$1a$ (0.952, 0.387, 0.620)
			$\beta= 67.735^\circ$	$1a$ (0.722, 0.093, 0.412)
			$\gamma= 113.245^\circ$	$1a$ (0.954, 0.578, 0.414)
				$1a$ (0.147, 0.840, 0.566)
				$1a$ (0.679, 0.344, 0.406)
				$1a$ (0.340, 0.707, 0.513)
				$1a$ (0.203, 0.290, 0.592)
				$1a$ (0.380, 0.826, 0.443)
				$1a$ (0.049, 0.096, 0.410)
				$1a$ (0.356, 0.344, 0.402)
				$1a$ (0.750, 0.146, 0.538)
				$1a$ (0.771, 0.741, 0.577)
				$1a$ (0.714, 0.835, 0.519)
				$1a$ (0.014, 0.842, 0.447)
				$1a$ (0.828, 0.600, 0.620)

Cmme-C48atom	<i>Cmme</i>	-8.12 eV	<i>a</i> = 7.769 Å	8 <i>m</i> (0.000, 0.866, 0.586)
			<i>b</i> = 5.872 Å	8 <i>m</i> (0.000, 0.634, 0.586)
			<i>c</i> = 24.000 Å	8 <i>m</i> (0.000, 0.366, 0.414)
			$\alpha$ = 90.000°	8 <i>m</i> (0.000, 0.134, 0.414)
			$\beta$ = 90.000°	8 <i>m</i> (0.500, 0.366, 0.586)
			$\gamma$ = 90.000°	8 <i>m</i> (0.500, 0.134, 0.586)
				8 <i>m</i> (0.500, 0.866, 0.414)
				8 <i>m</i> (0.500, 0.634, 0.414)
				8 <i>n</i> (0.088, 0.250, 0.606)
				8 <i>n</i> (0.912, 0.250, 0.606)
				8 <i>n</i> (0.412, 0.250, 0.394)
				8 <i>n</i> (0.588, 0.250, 0.394)
				8 <i>n</i> (0.912, 0.750, 0.394)
				8 <i>n</i> (0.088, 0.750, 0.394)
				8 <i>n</i> (0.588, 0.750, 0.606)
				8 <i>n</i> (0.412, 0.750, 0.606)
				16 <i>o</i> (0.844, 0.963, 0.419)
				16 <i>o</i> (0.656, 0.117, 0.486)
				16 <i>o</i> (0.656, 0.037, 0.419)
				16 <i>o</i> (0.844, 0.883, 0.486)
				16 <i>o</i> (0.156, 0.963, 0.419)
				16 <i>o</i> (0.344, 0.117, 0.486)
				16 <i>o</i> (0.156, 0.883, 0.486)
				16 <i>o</i> (0.344, 0.037, 0.419)
				16 <i>o</i> (0.656, 0.963, 0.581)
				16 <i>o</i> (0.844, 0.117, 0.514)
				16 <i>o</i> (0.844, 0.037, 0.581)
				16 <i>o</i> (0.656, 0.883, 0.514)
				16 <i>o</i> (0.344, 0.963, 0.581)
				16 <i>o</i> (0.156, 0.117, 0.514)
				16 <i>o</i> (0.344, 0.883, 0.514)
				16 <i>o</i> (0.156, 0.037, 0.581)
				16 <i>o</i> (0.344, 0.463, 0.419)
				16 <i>o</i> (0.156, 0.617, 0.486)
				16 <i>o</i> (0.156, 0.537, 0.419)
				16 <i>o</i> (0.344, 0.383, 0.486)
				16 <i>o</i> (0.656, 0.463, 0.419)
				16 <i>o</i> (0.844, 0.617, 0.486)
				16 <i>o</i> (0.656, 0.383, 0.486)
				16 <i>o</i> (0.844, 0.537, 0.419)
				16 <i>o</i> (0.156, 0.463, 0.581)

				$16o$ (0.344, 0.617, 0.514)
				$16o$ (0.344, 0.537, 0.581)
				$16o$ (0.156, 0.383, 0.514)
				$16o$ (0.844, 0.463, 0.581)
				$16o$ (0.656, 0.617, 0.514)
				$16o$ (0.844, 0.383, 0.514)
				$16o$ (0.656, 0.537, 0.581)
P1-C24atom	<i>P1</i>	-8.25 eV	$a= 5.529 \text{ \AA}$	$1a$ (0.856, 0.556, 0.450)
			$b= 6.890 \text{ \AA}$	$1a$ (0.293, 0.879, 0.475)
			$c= 25.054 \text{ \AA}$	$1a$ (0.602, 0.308, 0.448)
			$\alpha= 95.764^\circ$	$1a$ (0.195, 0.099, 0.479)
			$\beta= 91.554^\circ$	$1a$ (0.204, 0.224, 0.443)
			$\gamma= 68.269^\circ$	$1a$ (0.355, 0.334, 0.432)
				$1a$ (0.483, 0.738, 0.444)
				$1a$ (0.736, 0.759, 0.438)
				$1a$ (0.108, 0.457, 0.530)
				$1a$ (0.829, 0.129, 0.536)
				$1a$ (0.488, 0.581, 0.527)
				$1a$ (0.954, 0.862, 0.527)
				$1a$ (0.415, 0.898, 0.562)
				$1a$ (0.642, 0.704, 0.557)
				$1a$ (0.538, 0.227, 0.559)
				$1a$ (0.362, 0.108, 0.563)
				$1a$ (0.114, 0.449, 0.466)
				$1a$ (0.755, 0.124, 0.475)
				$1a$ (0.616, 0.517, 0.465)
				$1a$ (0.820, 0.911, 0.469)
				$1a$ (0.895, 0.678, 0.549)
				$1a$ (0.251, 0.801, 0.525)
				$1a$ (0.389, 0.426, 0.546)
				$1a$ (0.097, 0.219, 0.535)
P1-C8atom-2	<i>P1</i>	-7.54 eV	$a= 2.808 \text{ \AA}$	$1a$ (0.915, 0.663, 0.524)
			$b= 3.879 \text{ \AA}$	$1a$ (0.748, 0.744, 0.582)
			$c= 24.991 \text{ \AA}$	$1a$ (0.412, 0.452, 0.525)
			$\alpha= 90.533^\circ$	$1a$ (0.278, 0.377, 0.466)
			$\beta= 90.038^\circ$	$1a$ (0.464, 0.637, 0.438)
			$\gamma= 87.850^\circ$	$1a$ (0.572, 0.378, 0.582)
				$1a$ (0.656, 0.061, 0.601)
				$1a$ (0.951, 0.699, 0.459)
P1-C10atom	<i>P1</i>	-8.39 eV	$a= 3.610 \text{ \AA}$	$1a$ (0.130, 0.746, 0.441)
			$b= 3.641 \text{ \AA}$	$1a$ (0.722, 0.924, 0.570)

P1-14atom	<i>P1</i>	-8.11 eV	<i>c</i> = 25.409 Å	1 <i>a</i> (0.816, 0.234, 0.542)
			<i>a</i> = 110.138°	1 <i>a</i> (0.130, 0.093, 0.496)
			<i>β</i> = 86.011°	1 <i>a</i> (0.980, 0.670, 0.568)
			<i>γ</i> = 95.242°	1 <i>a</i> (0.110, 0.158, 0.437)
				1 <i>a</i> (0.369, 0.678, 0.559)
				1 <i>a</i> (0.432, 0.436, 0.430)
				1 <i>a</i> (0.810, 0.428, 0.432)
				1 <i>a</i> (0.453, 0.305, 0.526)
			<i>a</i> = 3.571 Å	1 <i>a</i> (0.857, 0.549, 0.528)
			<i>b</i> = 3.977 Å	1 <i>a</i> (0.828, 0.623, 0.596)

**Table S2.** The electronic effective mass ( $m_e$ ), hole effective mass ( $m_h$ ), and carrier mobility ( $\mu$ ) of electronic and hole along x and y direction ( $\text{cm}^2 \cdot \text{V}^{-1} \cdot \text{s}^{-1}$ ).

	$m_e$	$m_h$	$\mu_{xe}$	$\mu_{ye}$	$\mu_{xh}$	$\mu_{yh}$
2D diaphite	0.75	0.87	1031	560	1386	777
black phosphorus <sup>1</sup>	0.44	0.98	1110-1140	80	640-700	26
monolayer MoS <sub>2</sub> <sup>2</sup>	0.48	0.64			37-311	
Si	1.02	0.87			~1400	

## REFERENCE

- (1) Qiao, J.; Kong, X.; Hu, Z. X.; Yang, F.; Ji, W. High-Mobility Transport Anisotropy and Linear Dichroism in Few-Layer Black Phosphorus. *Nat. Commun.* **2014**, *5*, 4475.
- (2) Yun, W. S.; Han, S. W.; Hong, S. C.; Kim, I. G.; Lee, J. D. Thickness and Strain Effects on Electronic Structures of Transition Metal Dichalcogenides: 2H-MX<sub>2</sub> Semiconductors (M=Mo, W; X=S, Se, Te). *Phys. Rev. B* **2012**, *85*, 033305.